LAWRENCE
LIVERMORE
NATIONAL
LABORATORY

LLNL-CONF-583412

Theory and Simulations of ELM Control with a Snowflake Divertor

D. D. Ryutov, R. H. Cohen, E. Kolemen, L. LoDestro, M. Makowski, J. Menard, T. D. Rognlien, V. A. Soukhanovskii, M. V. Umansky, X. Q. Xu

September 20, 2012

International Atomic Energy Agency Fusion Energy Conference
San Diego, CA, United States
October 8, 2012 through October 13, 2012

Disclaimer

Theory and Simulations of ELM Control with a Snowflake Divertor

D.D. Ryutov[1], R.H. Cohen[1], E. Kolemen[2], L. LoDestro[1], M. Makowski[1], J. Menard[2], T.D. Rognlien[1], V.A. Soukhanovskii[1], M.V. Umansky[1], X. Xu[1]

[1]*Lawrence Livermore National Laboratory, Livermore, CA 94551, USA*
[2]*Princeton Plasma Physics Laboratory, Princeton, NJ 08450, USA*

E-mail contact: ryutov1@llnl.gov

Abstract. A snowflake divertor (SF) offers an attractive solution to the problem of heat exhaust in tokamaks. The poloidal magnetic field null in the snowflake divertor is of second order, i.e., the poloidal field is proportional to the second power of the distance from the null, not the first power as in a standard X-point divertor ("standard null"=SN). An obvious feature of the SF configuration is a much stronger flux expansion near the null and related changes in the edge plasma behavior compared to the SN. Our paper is concerned with the use of a snowflake (SF) divertor for significant reduction of the pulsed heat loads produced by edge localized modes (ELMs). Main attention is paid to the identification of the effects that can reduce the divertor heat load once the ELM had occurred. Such effects include enhanced convection in the area of a very weak poloidal field characteristic of the SF divertor, and temporal dilation of the heat pulse during the ELM event. Their combined effect can lead to a more than 10-fold decrease of the pulsed heat loads on divertor plates. In an attempt to better understand the other part of the problem, the possibility of controlling ELM occurrence, simulations of the pedestal instability and plasma transport in scrape-off layer (SOL) of the near-snowflake configuration have begun.

1. Introduction

During ELM events, a significant fraction of the stored plasma energy is dumped into the scrape-off layer and quickly reaches divertor targets [1, 2]. Under reactor-relevant conditions, this may cause a pulsed increase of the surface temperature to a level where melting of the surface layers would occur. There exist several techniques for the mitigation of ELM-induced damage. In particular, imposing resonant magnetic perturbations by special in-vessel coils can lead to significant reduction of the ELMs amplitude [3]. Another recently identified mitigation technique is based on the use of favorable properties of a snowflake divertor geometry [4]: weakness of the poloidal field in a larger (than in a standard divertor) volume, the appearance of four strike points, and increased connection length [5-7]. In studies [5-7] as well as in the present paper the origin of ELMs is not discussed and they are treated as pulsed sources of particles and heat for the SOL. We then consider the further redistribution of heat in the SOL as it approaches the target plates. We do not consider the effect of the divertor geometry (snowflake vs. standard) on the generation of ELMs, although such an effect also exists as was shown in experiments on tokamaks TCV and NSTX [8-10]. Some first numerical simulations of this effect using the BOUT++ code are briefly discussed in Sec. 4 below.

In Sec. 2 we study the effect of enhanced plasma convection around the PF null point. Convection can be driven by the loss of MHD equilibrium [5, 7], excitation of ballooning modes in the divertor region, and by flute-like instabilities affected by strong magnetic shearing [11, 12]. In Sec. 3 we proceed to the effect of temporal dilation of the ELM heat pulse [6] by the increased connection length and find that this effect can be substantial. In Sec. 4 we present simulation of pedestal stability for a near-snowflake geometry, which is a step towards understanding of the role of the divertor geometry on the process of ELM generation. In Sec. 5, initial results of numerical studies of effects of SF enhanced magnetic shearing on resistive ballooning (RB) modes are presented. Sec. 6 contains a brief summary.

2. Plasma convection near the null-point.

2.1 Convection driven by the loss of equilibrium at low poloidal field

In the snowflake (or near-snowflake) geometry, the poloidal magnetic field strength scales quadratically with the distance d from the (second-order) null, $B_P = CB_{PM}\left(d/a\right)^2$, where a is the minor radius, B_{PM} is the poloidal field strength in the outer midplane, and C is a numerical coefficient of order one depending on the details of the geometry. When the particles and energy ejected from the main plasma during an ELM burst reach the vicinity of the null-point, the plasma pressure rapidly increases, as does the parameter β_P, the ratio of the plasma pressure to the pressure of the poloidal magnetic field. In Refs. [5, 7] it was conjectured that formation of the zone of a high β_P should lead to the onset of convection driven by the toroidal curvature $1/R$, with R being a major radius corresponding to the PF null. For parameters typical of an ITER-scale fusion facility and an ELM energy release corresponding to a few percent of the stored energy, the size of the zone of $\beta_P > 1$ is substantial, d~40 cm. Estimates of the turn-over time for the rolls formed in the low-poloidal-field region have shown [5] that the plasma is convected between all four divertor legs, and the plasma width in each of them becomes greater than in a standard divertor by a factor of a few. Convection involves only the area around the PF null; the subsequent plasma flow along the divertor legs occurs in a regular fashion, guided by a weakly perturbed (essentially vacuum) poloidal field.

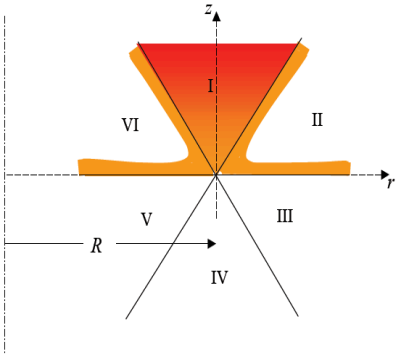

FIG. 1 Snowflake divertor configuration in the mode typical for a standard divertor, where the plasma pressure in the private flux region is small. In the snowflake case the private flux region occupies sectors III-V. The weak poloidal field of the snowflake cannot provide such an equilibrium and gets strongly distorted and swept into the private flux zone. One can conjecture that plasma convection should ensue in the zone defined by Eq. (3) and shown as a rough sketch in Fig. 2. The dash-dotted line at the left is the geometrical axis, and R is the major radius at the PF null.

Here we consider the issue of the loss of equilibrium in a more quantitative fashion. We use a model in which the plasma pressure p is constant along the flux surfaces, at least in the vicinity of the null. In the absence of convection or other mechanisms for rapid cross-field transport in the divertor area, the plasma populates flux surfaces directly connected to the midplane SOL (Fig. 1). The equilibrium is toroidally symmetric, with poloidal current determined from the force-balance equation, $\boldsymbol{j}_P = (c/B_T^2)(\boldsymbol{B}_T \times \nabla p) + (\boldsymbol{B}_P / B_T) j_T$, where j_T is the equilibrium toroidal current which depends on both r and z. The condition that the divergence of the equilibrium current is zero, $\nabla \cdot \boldsymbol{j}_P = 0$, reads as

$$\frac{2c}{B_T R}\frac{\partial p}{\partial z} + (\boldsymbol{B}_P \cdot \nabla)\left(\frac{j_T}{B_T}\right) = 0 \qquad (1)$$

In the vicinity of the divertor null, the toroidal magnetic field can be considered as constant and therefore drops out from the equilibrium condition. The poloidal flux function Φ, satisfying

$B_z = \partial\Phi / \partial r$; $B_r = -(1/r)\partial\Phi / \partial z$, is related to toroidal current density by Ampere law, $\nabla^2\Phi = 4\pi j_T / c$.

Based on Eq. (1), we can write the following estimate for the toroidal current density at the distance d from the second-order null: $j_T \sim 2cp / B_P R$. Then Ampere's law yields an estimate of the distortion of the vacuum poloidal magnetic field:

$$\Delta B_P / B_P \sim 8\pi pd / RB_P^2 . \qquad (2)$$

For a pressure distribution of the type shown in Fig. 1, where the gradient is directed across the horizontal branches of the separatrix, with the pressure decreasing towards the private flux region, the perturbation of the PF configuration will allow the plasma to populate a significant portion of the formerly private flux.

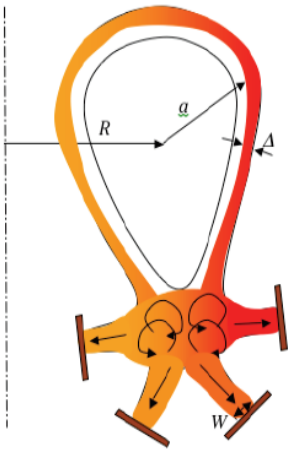

FIG.2 The width W of the wetted area on each target is several times greater than that for the standard divertor; together with activation of 4 strike points this may lead to ~ 10-fold reduction of the heat flux.

The condition of loss of vacuum equilibrium, $\Delta B_P > B_P$, can be represented as

$$\beta_{PM} > C^2 (R/a)(d/a)^3 , \qquad (3)$$

where $\beta_{PM} \equiv 8\pi p / B_{PM}^2$ and we have used the aforementioned expression $B_P = CB_{PM}(d/a)^2$ for the poloidal field. For C~1, d/a~1/15, R/a=2.5, the poloidal beta required for spreading of the plasma over the private flux region is less than 10^{-3}, whereas type 1 ELMs produce the poloidal beta ~ 10^{-2}. The estimate of the size of the affected zone is somewhat smaller than that suggested in Refs. [5. 7], where there was no parameter d/R in the right-hand side of equation (2). On the other hand, the presence of the high power of d/a in the right-hand side of Eq. (3) makes the estimate of the zone of lost equilibrium insensitive to the presence of this additional factor. If one wants to further increase the size of this zone, one has to select the field geometries with C<1.

The plasma convection that ensues if condition (3) holds by some margin leads to heat-flux partitioning between all four strike points, as well as to a broadening of the wetted zone in each strike point, as shown in Fig. 2. In the absence of this convective broadening, the heat-flux distribution in each strike point has a characteristic shape with a very sharp drop towards the private flux region and smoother decrease in the opposite (outward) direction. The convection should cause roughly symmetric broadening, with the heat-flux imprint half-width the same for the private and common flux regions. This would be an experimental signature of the anomalous broadening occurring in the divertor.

The convection would have the shape of toroidally-symmetric rolls. It will lead to perturbations of the poloidal field and, possibly, to reconnection events in the affected area.

2.2 Convection driven by ballooning modes

One more effect related to the weakness of the poloidal field is development of ballooning modes in the areas where the pressure gradient has a component directed towards the geometrical axis (Fig. 3). Due to the weakness of the poloidal field, the distance between two successive intersections of the field line with the poloidal plane is small,

$\delta \sim 2\pi R(B_P / B_T) \sim (2\pi Ca / q^*)(d / a)^2$, with $q^* \equiv aB_T / RB_{PM} \sim 5$. This leads to the possibility of development of ballooning modes in the divertor, despite the smallness of $\beta_T \equiv 8\pi p / B_T^2$. Indeed, for small-enough d, the field line can make $N = d / \delta \sim a / d$ turns staying in the area of the destabilizing curvature (we assume that $2\pi C / q^* \sim 1$). With that, the energy principle [13] leads to the following estimate for the instability criterion for ballooning modes:

$$\beta_T > \frac{d^3}{2a^2 R}. \qquad (4)$$

For $\beta_T \sim 10^{-3}$ typical for an ELM event and for a standard aspect ratio of R/a=2.5, this condition is satisfied for d/a<1/15. When writing this estimate we assume that the gradient length scale is comparable to the distance d; if it is shorter, the critical beta decreases in proportion to the length scale.

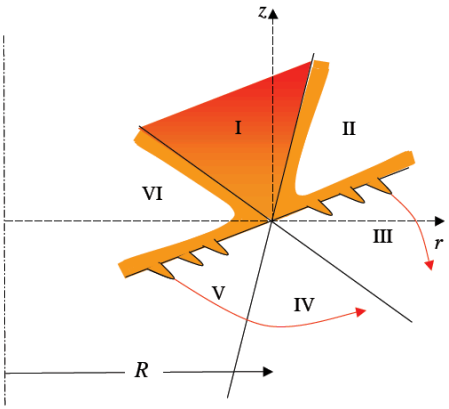

Fig. 3 For a specific orientation of the snowflake branches, the plasma would populate the private flux region and all strike points by a ballooning instability. The desired orientation corresponds to the destabilizing projection of the toroidal curvature on the pressure gradient at the boundary of a private flux region. Instability develops if condition (4) is satisfied. As the ballooning modes have high growth rate, the plasma, before reaching divertor targets (not shown), fills both sectors V and IV (coming from the inboard side) and sector III (coming from the outboard side).Thereby all 4 strike points are engaged, with significant broadening of the wetted zone in each strike point.

The ballooning instability would lead to broadening of only those interfaces for which the pressure gradient is properly oriented with respect to the toroidal curvature. In the geometry of Fig. 1, this would not occur at the interface of the private and common flux regions. It would, however, occur for the snowflake orientation shown in Fig. 3. In this regard the ballooning-driven convection differs from the convection driven by the loss of equilibrium which would lead to the overall mixing in the affected area, irrespective of what was the direction of the initial gradient.

2.3. Flute modes

One more possible group of instabilities is flute-like electrostatic (or almost electrostatic) instabilities that are not accompanied by perturbation of the magnetic field and can therefore exist even in a zero-pressure plasma. Instability of these modes in the divertor area is associated with the absence of complete line-tying on the divertor plates [14]; these modes are also strongly affected the magnetic shear in the vicinity of the PF null [15] that allows for enhanced resistive (electrostatic) ballooning of the modes [16]. In the presence of across-field electron temperature gradient these modes can develop even in the case where the curvature has a stabilizing effect [11], although their growth rate is smaller. The presence of magnetic shear in the neighborhood of the x point suppresses penetration of such modes across the x-point region and so tends to divide modes into those localized in the main SOL and in the divertor [15]. We have analyzed such modes in the past through the use of a heuristic boundary condition in the neighborhood of the x point [see, e.g. Ref. 11]; we have re-examined this boundary condition for the snowflake divertor and find it to be essentially unchanged from the conventional case. Residual differences

can be absorbed as in Ref. [11] into a factor G multiplying the heuristic impedance; from the dispersion relation obtained in Ref. [11] the effect of G on instability frequencies is weak. Hence the primary effects of the snowflake configuration on these instabilities are (a) via their parametric dependence on the connection length (distance along the field line to the null region) and (b) the increased field line length across the x-point region contributing to increased disconnect of modes across this region. This analysis will be described in more detail in a separate publication.

3. Temporal dilation of ELM heat pulse

The larger region of very low B_p near the magnetic null for the SF configuration (compared to the standard X-point divertor) leads directly to a longer distance along the magnetic field between the outer equatorial midplane region and the divertor plates near the separatrix. Consequently, because the ELM energy and density perturbations are ejected into the scrape-off layer around the midplane, the time for these perturbations to reach the plates is longer for SF, resulting in a lower peak heat-flux at the divertor and less surface heating. In addition, the SF can have a larger poloidal flux expansion. A quantitative assessment of these effects is obtained from time-dependent simulations of the ELM heat flux on the divertor plate using the UEDGE edge transport code [17]. Two-dimensional fluid equations are used for the plasma density, ion parallel velocity, and electron and ion temperatures. The recycling neutrals are described by fluid continuity and parallel momentum equations, with multi-step ionization and recombination processes included. The simulations are performed beginning with a model MHD equilibrium of the Fusion Development Facility (FDF) design [18], and then modifying the poloidal field coil currents to produce a SF-plus configuration. The two magnetic equilibria are illustrated by the flux-surface computational meshes shown in Fig. 4. Beginning from a steady-state edge/SOL plasma, both configurations are simulated with an additional "ELM" energy source of 40 kJ ejected over a 200 μs pulse near the midplane separatrix, mostly in the SOL. Figure 5 compares the profile of the heat-flux on the outer divertor near the peak of the heat flux (200 μs) for the standard and SF divertor configurations. Also shown is the radial profile of the up-stream ELM source mapped along flux surfaces to the divertor plate. The SF divertor has less than ½ the peak heat-flux compared to the standard case. The wider mapped source profile for the SF case shows that a portion of the heat flux reduction in this case is from flux expansion, but additionally, there is substantial spreading

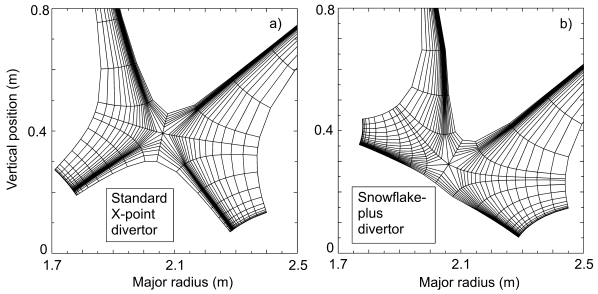

FIG. 4 UEDGE flux-surface mesh used for standard and SF-plus FDF ELM simulations; from Ref. [6].

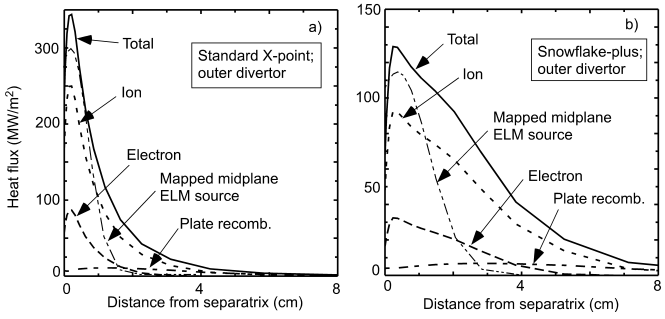

FIG. 5 Heat-flux on outer plates at 200 μs for standard & SF cases: from Ref. [6].

beyond the source profile indicating the time-dilation effect. The possible loss-of-equilibrium and/or simple curvature-driven instabilities arising from the extended low-β_p region should further reduce the peak heat for the SF case.

4. Effect of the snowflake geometry on the pedestal ballooning modes

The ELM simulations in this paper were done with a three-perturbation-field (magnetic flux $\tilde{A}_{||}$, electric potential $\tilde{\Phi}$, and pressure $\tilde{p}$) model [19]. A non-ideal effect - finite parallel viscosity is retained for numerical reason near the x-point due to strong lower triangularity. The three-field equations are solved using a field-aligned (flux) coordinate system with shifted radial derivatives on a periodic domain in toroidal angle and in the parallel coordinate (with a twist-shift periodic boundary condition).

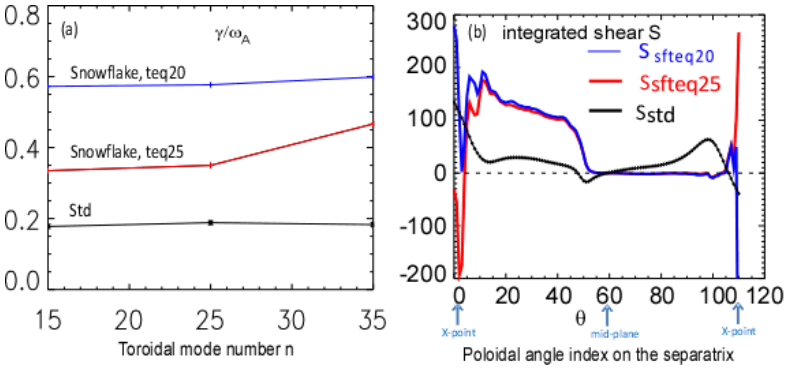

FIG. 6. (a) The influence of the divertor null on the linear growth rate of P–B modes versus toroidal mode number n for the standard LSN (black), and SF with distance 25cm (red) and 20 cm (blue) between two nearby x-points; (b) The integrated magnetic shear S along the poloidal index on the magnetic separatrix, $S=\int_{\theta_0}^{\theta} IJ/R^2 d\theta$, where $I(\psi)=RB_T$, R is the tokamak major radius, B_T is the toroidal magnetic field, and J is the coordinate Jacobian.

In order to study the divertor null effects, the BOUT++ ELM simulations were run with both standard lower single-null (LSN) and snowflake (SF) equilibrium plasma shapes. The plasma profiles are taken from experimental measurements in DIII-D ELMing H-mode [20]. The lower single-null (LSN) equilibrium is generated by the kinetic EFIT code. The snowflake (SF) equilibria are generated by TEQ and match the EFIT plasma boundary except near the lower x-point. Steady-state conditions during the ELMing H-mode phase were I_p = 1.5 MA, B_T = 1.95 T, average P_{NBI} = 5.6 MW, R = 1.75 m, a = 0.6 m, $\kappa = 1.82, \delta = 0.65$, $q_{95} = 3.64$, and $\beta_N = 2.0$.

The initial results of linear simulations of peeling–ballooning (P-B) modes are shown in the Fig. 6(a) for the normalized growth rate vs. toroidal mode number n, with $\omega_A = 6.77 \times 10^6 s^{-1}$ being the normalization frequency. We find that (1) the divertor null has significant impact on the peeling-ballooning mode due to the integrated magnetic shear S, as shown in Fig. 6(b); (2) the linear growth rate increases from the standard LSN to snowflake divertor; the growth rate further increases when the distance between two nearby x-point in snowflake configuration decreases. Figure 6(b) shows that the integrated magnetic shear S decreases from the standard LSN to snowflake divertor in the outer lower half of tokamak near the x-point and increases in the inner half of tokamak. This is possibly due to the strong lower triangularity of plasma shape. The growth rate changes are possibly due to the decrease of the magnetic shear in the outer half of tokamak, particularly near the x-point, where the P-B mode is localized. It should be noted, however, that a larger growth rate does not necessarily lead to a larger ELM size, as shown in Fig.10 of Ref. 21.

5. Electrostatic edge instabilities in the presence of enhanced shear

Resistive ballooning (RB) instabilities are of interest because they are relevant to edge plasma turbulence. Here we are reporting results of initial calculations with the BOUT++ code investigating the effects of SF enhanced magnetic shear on the linear growth rates of electrostatic RB instability [22].

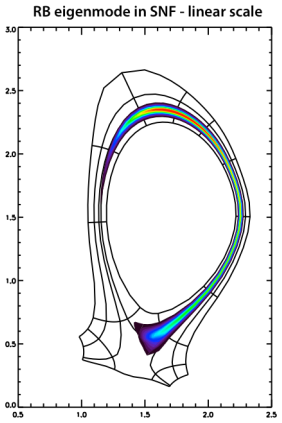

FIG.7 Spatial form of RB n=100 eigenmode in edge plasma region for parameters of DIII-D tokamak. A few grid lines are shown to illustrate magnetic geometry.

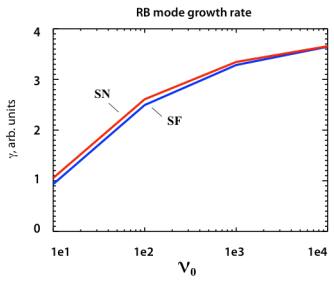

FIG. 8. The influence of the divertor null on the linear growth rate of electrostatic RB mode is shown. The mode growth rate is plotted vs. collisionality scaling parameter ν_0

In our calculations it is found that curvature-driven RB modes with toroidal mode number n=100 (characteristic of edge plasma turbulence) don't extend poloidally far enough to be strongly influenced by the PF null region. The explanation is as follows. The poloidal extent of the mode is controlled by the integrated magnetic shear accumulated between the midplane and lower divertor. For parameters used in these calculations (corresponding to DIII-D tokamak) the integrated shear is strong enough to attenuate the mode poloidally before it can "feel" the PF null region. This is illustrated by the spatial form of RB eigenmode for parameters of DIII-D tokamak, shown in Fig. 6. For smaller mode numbers and/or smaller plasma collisionality the eigenmode poloidal span becomes broader, which makes the mode more sensitive to the details of the PF null region. Fig. 7 shows the growth rate vs. the collisionality scaling parameter. For smaller collisionality the effects of SF on the growth rate become noticeable.

6. Summary and discussion

In summary, we have identified and analyzed several effects that may inform the analysis of existing data and planning for further experiments with SF divertors: 1) The onset of curvature-driven convection in the divertor area; 2) Significant temporal dilation of heat pulses during ELM events; 3) The presence of a noticeable effect of the transition to a snowflake geometry on the growth rate of pedestal peeling-ballooning modes. We have also started full-geometry simulations of the electrostatic edge turbulence.

Some of the effects discussed in this paper have already been observed experimentally. In particular, the effect of the changed geometry on the ELM amplitude and frequency has been observed on the NSTX and TCV tokamaks [8-10]; see also posters 453-EX/P5-21, 490-EX/P5-22 at this conference. Activation of additional strike points has also been seen at both of these devices. Effect of symmetrization of the plasma imprint in the strike-point zones indicating the anomalous broadening in the divertor area (discussed in Sec. 2.1 above) has been seen on the

TCV facility [23]. The heat-deposition profile observed on NSTX [9, 10] also points at the presence of this additional broadening on the top of a simple flux expansion in the common-flux area.

These effects occur on the background of significant reduction of the overall divertor heat fluxes caused by the enhanced flux expansion and radiative losses during the inter-ELM periods [9, 10], pointing at significant potentialities for the snowflake divertor as a solution for the heat exhaust problem in tokamaks.

Acknowledgments

We are grateful to Dr. B. Cohen (LLNL) for helpful discussions. Work performed for U.S. DoE by LLNL under Contract DE-AC52-07NA27344 and LDRD project 11-ERD-058, and by PPPL under Contract DE-AC02-09CH11466.

References.

1. HILL, D.N., J. Nuclear Materials **241-243** (1998) 182.
2. LOARTE, A., LIPSCHULTZ, B. , KUKUSHKIN, A. et al, Nucl. Fusion **47** (2007) S203.
3. EVANS, T.E., MOYER, R.A., THOMAS, P.R. et al. Phys. Rev. Lett., **92** (2006) 235003.
4. RYUTOV, D.D., Phys. Plas., **14** (2007) 064502.
5. RYUTOV, D.D., COHEN, R.H., ROGNLIEN, T.D., UMANSKY, M.V., Contrib. Plasma Phys., **52** (2012) 539.
6. ROGNLIEN, T.D., COHEN, R.H., RYUTOV, D.D., UMANSKY, M.V., To appear in J. Nucl. Mat., 2012.
7. RYUTOV, D.D., COHEN, R.H., ROGNLIEN, T.D., UMANSKY, M.V., Submitted to PPCF, 2012.
8. PIRAS, F., S. CODA, S., DUVAL, B.P., et al. PRL, **105** (2010) 155003.
9. SOUKHANOVSKII, V.A., AHN, J.-W., BELL, R. E., et al., Nucl. Fus., **51** (2011) 012001.
10. SOUKHANOVSKII, V.A., BELL, R. E., DIALLO, A., et al. Phys. Plasmas, **19**, 082504, 2012.
11. COHEN, R.H., LABOMBARD, B., RYUTOV, D.D., et al., Nucl. Fusion, **47** (2007) 612.
12. RYUTOV, D.D., COHEN, R.H., Contrib. Plasma Phys., **48** (2008) 48.
13. BERNSTEIN, I. B., FRIEMAN, E. A., KRUSKAL, M. D., KULSRUD, R. M., Proc. R. Soc. London, Ser. A **244** (1958)17.
14. BERK, H.L., COHEN, R.H., RYUTOV, D.D. et al., Nuclear Fusion, **33** (1993) 263.
15. FARINA, D., POZZOLI, R., RYUTOV, D.D., Nuclear Fusion, **33** (1993) 1315.
16. XU, X.Q., COHEN, R.H., ROGNLIEN, T.D., MYRA, J.R., Phys. Plasmas, **7** (2000) 1951.
17. ROGNLIEN, T. D., MILOVICH, J.L., RENSINK, M.E., PORTER, G.D., J. Nucl. Mat. **196** (1992) 347.
18. A.M. GAROFALO, V.S. CHAN, R.D. STAMBAUGH et al. IEEE Trans. Plasma Sci. **38**, 461 (2010)
19. XU, X.Q., DUDSON, B., SNYDER, P.B., et al., Phys. Rev. Lett. **105** (2010) 175005.
20. FENSTERMACHER, M., et al., submitted to J. Nuclear Mat.
21. XI, P.W., XU, X.Q., WANG, X.G., XIA, T.Y., Phys. Plasmas, **19** (2012) 092503.
22. CARRERAS, B.A., GARCIA, L., DIAMOND, P.H., et al. Phys. Fluids, **30** (1987)1388.
23. LABIT, B., REIMERDES, H., VIJVERS, W. et al., Paper P5.091, 39th EPS Conference on Plasma Physics and Controlled Fusion, Stockholm, 2012.